

The Scattered Light Time-history Diagnostic Suite at the National Ignition Facility

M. J. Rosenberg,^{1, a)} J. E. Hernandez,² N. Butler,² T. Filkins,¹ R. E. Bahr,¹ R. K. Jungquist,¹ M. Bedzyk,¹ G. Swadling,² J. S. Ross,² P. Michel,² N. Lemos,² J. Eichmiller,² R. Sommers,² P. Nyholm,² R. Boni,¹ J. A. Marozas,¹ R. S. Craxton,¹ P. W. McKenty,¹ A. Sharma,¹ P. B. Radha,¹ D. H. Froula,¹ P. Datte,² M. Gorman,² J. D. Moody,² J. M. Heinmiller,³ J. Fornes,³ P. Hillyard,³ and S. P. Regan¹

¹⁾Laboratory for Laser Energetics, University of Rochester, Rochester, NY 14623, USA

²⁾Lawrence Livermore National Laboratory, Livermore, CA 94550, USA

³⁾Nevada National Security Site, Livermore, CA 94551, USA

(Dated: 15 February 2021)

The Scattered Light Time-history Diagnostic (SLTD) is being implemented at the National Ignition Facility (NIF) to expand greatly the angular coverage of absolute scattered-light measurements for direct- and indirect-drive inertial confinement fusion (ICF) experiments. The SLTD array will ultimately consist of 15 units mounted at a variety of polar and azimuthal angles on the NIF target chamber, complementing the existing NIF backscatter suite. Each SLTD unit collects and diffuses scattered light onto a set of three optical fibers, which transport the light to filtered photodiodes to measure scattered light in different wavelength bands: stimulated Brillouin scattering (350 to 352 nm), stimulated Raman scattering (430 to 760 nm), and $\omega/2$ (695 to 745 nm). SLTD measures scattered light with a time resolution of ~ 1 ns and a signal-to-noise ratio of up to 500. Currently, six units are operational and recording data. Measurements of the angular dependence of scattered light will strongly constrain models of laser energy coupling in ICF experiments and allow for a more robust inference of the total laser energy coupled to implosions.

I. INTRODUCTION

Measurements of scattered laser light are important diagnostics of laser energy coupling and laser-plasma instabilities (LPI)¹ in inertial confinement fusion (ICF)² experiments. Scattered light due to stimulated Brillouin scattering (SBS)³ represents a loss of laser energy that would otherwise drive the imploding capsule in direct-drive ICF⁴ or the *hohlraum* in indirect-drive ICF.⁵ Scattered light due to stimulated Raman scattering (SRS)⁶ or two-plasmon decay (TPD)⁷ may be an additional energy-loss mechanism and can also signify the presence of a suprathermal electron population that can preheat the capsule and degrade implosion performance.

At the National Ignition Facility (NIF),⁸ the scattered-light diagnostic suite⁹ originally consisted of two full-aperture backscatter stations (FABS) within two quads (closely clustered collections of four beams), one at 30° and one at 50° from the south pole of the target chamber, as well as near-backscatter imager (NBI) scatter plates surrounding each FABS and an additional NBI at 23° . Each FABS provides absolute time-resolved SBS and SRS scattered-light power and spectral measurements. (In this work, “SBS” is understood to include unabsorbed light near 351 nm.) NBI produces time-integrated images of SBS and SRS scattered light near the chamber wall and the time-resolved SRS spectrum at 23° . Additionally, the drive diagnostics (DrDs)¹⁰ measure time-resolved SBS light in 57 beam ports, although this is

useful predominantly on indirect-drive experiments on which there is significant light scattered directly back up the beamline. Overall, existing scattered-light measurements are confined to limited beam-port locations.

This diagnostic placement is predicated on the assumptions that scattered light is predominantly backscatter, symmetric about the NIF equator, and the same for each beam at a given polar angle. However, recent experiments have demonstrated the importance of multiple-beam effects¹¹ and sidescatter^{12,13} for SRS in both direct and indirect drive. Furthermore, polar-direct-drive (PDD) experiments¹⁴ are predicted to produce scattered light predominantly outside of beam ports and with significant variation as a function of polar and azimuthal angle. Indirect-drive implosions appear to suffer from a weaker x-ray drive than predicted,¹⁵ which is attributed to unexplained reduced laser coupling. It is plausible that scattered light not directed into beam ports, and therefore not observed by the existing scattered-light diagnostic suite, can explain this loss of laser energy.

These considerations motivate additional scattered-light measurements between beam ports to infer the total scattered-light distribution. Therefore, the Scattered Light Time-history Diagnostic (SLTD) has been developed to measure the time-resolved scattered light in three different wavelength bands – 350 to 352 nm (SBS), 430 to 760 nm (SRS), and 695 to 745 nm ($\omega/2$, corresponding to SRS or TPD-related scattered light at the quarter-critical density) – at 15 locations around the NIF target chamber outside the beam port envelope. Figure 1 shows the simulated¹⁶ distribution of SBS light in an example PDD implosion, the locations of NIF beam ports, including the existing FABS diagnostics, and the loca-

^{a)}Electronic mail: mros@lle.rochester.edu

tions of the SLTD suite. At present, six SLTD units are operational, providing data on SBS, SRS, and/or TPD instabilities to constrain models of laser-energy coupling in ICF experiments and to characterize potential hot-electron-generating instabilities.

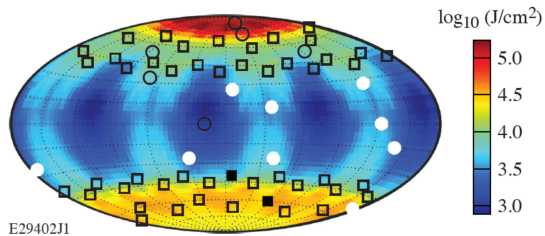


FIG. 1. Simulated distribution of SBS scattered light for a PDD experiment with cone swapping and wavelength detuning overlaid with the NIF quad port map (squares).¹⁶ Polar angle θ varies from 0 (top) to 180° (bottom), while azimuthal angle ϕ varies from 0 (left) to 360° (right). Existing FABs are located in two quads (solid black), while SLTDs [six implemented (black circles) and nine to be installed (white circles)] are located over a wide range of polar and azimuthal angles outside of beam ports.

II. INSTRUMENT DESIGN

Key SLTD measurement requirements are summarized in Table I. Absolute and relative calibration accuracy for scattered-light energy and power measurements is desired to better than $\pm 15\%$ in order to resolve angular-dependent scattered-light variations and for inference of total scattered light. A time resolution (10% to 90% rise time) of better than 1.5 ns is needed to resolve temporal variation of scattered light over laser pulses of 5- to 10-ns duration. A signal to noise ratio of >100 is desired to provide sufficient dynamic range and measurement accuracy. Minimum incident light fluence onto SLTD of $\sim 2 \times 10^4$ W/cm² is equivalent to a 4π averaged scattered-light power of 0.1 TW, of order 0.1 to 1% scattered light for low-power direct-drive experiments.^{12,16}

TABLE I. Key SLTD measurement requirements.

Requirement	Value
Absolute calibration accuracy	$<15\%$
Time resolution	<1.5 ns
Signal/noise	>100
Minimum signal	4×10^4 W/cm ² (SBS)
	2×10^4 W/cm ² (SRS)
	5×10^3 W/cm ² ($\omega/2$)

The SLTD optical hardware is mounted on diagnostic ports outside the NIF chamber wall. A schematic of the optical components is shown in Fig. 2. Light enters

SLTD through a set of vacuum and debris windows and is incident on a Labsphere Zenith optical diffuser after being apertured down to a diameter of 5.08 cm. The 250- μ m-thick diffuser, which is located ~ 590 cm from target chamber center (TCC), disperses the light forward in a near-Lambertian distribution with a transmission around 0.2. Three step-index optical fibers are positioned 20 cm from the diffuser, with a numerical aperture of 0.22 and a 400- μ m core diameter. The light is contained within a light tube coated black on the interior to minimize multiple reflections. Dimensions were chosen so that the fibers capture light from the entire surface of the diffuser and that the light fluence on the fibers is reduced to below damage thresholds.

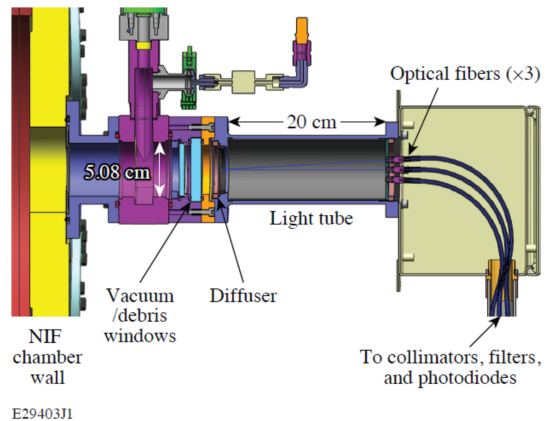


FIG. 2. Schematic of the SLTD optical components mounted behind the NIF chamber wall. Light passes through a 5.08-cm aperture onto a transmissive optical diffuser. Three optical fibers at the back of the light tube collect light from the entire area of the diffuser and relay the light to a separate box housing the optical collimators, filters, and photodiodes.

The light is transported through 2 m of fiber and relayed by a collimator through a set of filters that differentiate the three channels. The fiber length is limited (<5 m) to minimize chromatic dispersion ($\lesssim 100$ ps) in the broadband SRS channel. The SBS channel contains a narrowband filter to isolate light between 325 and 375 nm, although the predominant signal is from light that falls within $\sim \pm 1$ nm of the incident laser wavelength of 351 nm (frequency tripled from 1053 nm). The filter transmission at 351 nm is 0.52. The SRS channel is filtered by a bandpass filter, allowing light between 430 and 760 nm at a transmission of 0.96. The SRS channel is additionally filtered by a “notch” filter centered around 532 nm, which reduces unconverted second-harmonic (527 nm) light by more than four orders of magnitude, and a flattening filter with a wavelength-dependent transmission (0.1 at 532 nm). The flattening filter was custom-designed to compensate for the wavelength-dependent transmission of the diffuser and sensitivity of the photodiode so that the measurement is insensitive to the spectrum, which is not measured by SLTD. The $\omega/2$ channel is filtered by a pair of long- and short-pass filters that

permits light at wavelengths between 695 and 745 nm at a transmission of 0.95. Neutral density (ND) filters are also used to control light fluence on the photodiodes and are calibrated at the appropriate wavelength. The collimators were chosen so that the projected beam underfills the 10-mm-diameter active area of the photodiodes. The collimator transmission was measured to be 0.78 at 351 nm, 0.87 at 532 nm, and estimated to be 0.89 at 702 nm.

Hamamatsu R1328U-52 and R1328U-53 fast photodiodes, with 60-ps rise and 90-ps fall times, detect the light over the wavelength bands of interest. Photodiode sensitivity ranges from ~ 65 mA/W at 351 nm for the SBS channel to ~ 4 mA/W at 730 nm for the SRS and $\omega/2$ channels. Current from the photodiodes is carried by coaxial cables (LMR400 or LMR600) over a distance of 35 to 65 m to a Tektronix MSO58LP 1-GHz digitizer with 12-bit resolution. The digitizer response determines the temporal resolution of SLTD.

III. CALIBRATION AND PHOTOMETRICS

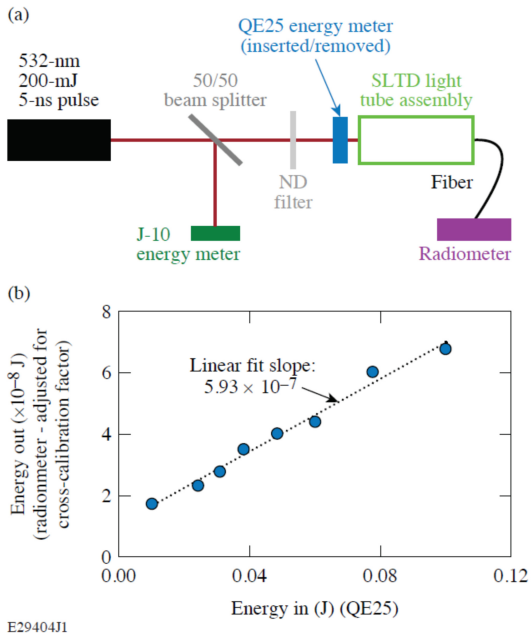


FIG. 3. (a) Schematic and (b) results of SLTD light tube integrated calibration. The QE25 measured light energy incident on SLTD, while the radiometer measured light energy exiting the fiber. Neutral density (ND) filters were placed in front of SLTD to vary the incident energy. The J-10 energy meter monitored the stability of the laser output. After correcting for the cross-calibration of the energy meters, the SLTD transmission at 532 nm was determined to be 5.93×10^{-7} .

The integrated transmission of the SLTD light tube assembly, including the vacuum and debris windows, diffuser, light tube, and optical fibers, was calibrated using a 532-nm, 200-mJ, 5-ns pulsed source. The calibration setup is shown in Fig. 3(a). A beamsplitter divided the

laser energy between a beam propagating forward into SLTD and a beam propagating into a Coherent J-10 energy meter that served as a reference for the stability of the laser output. The energy measured in this reference leg was nearly constant, with a relative standard deviation of 0.5%. The energy in the beam incident on SLTD was measured with a Gentec QE25 energy meter, which is used as the absolute energy reference. When this meter was removed, the energy emerging from one of the SLTD fibers was measured by a radiometer, of order 10 nJ. Various ND filters (up to ND1.0) were placed in front of SLTD to vary the incident laser energy in order to measure the coefficient between energy into SLTD and energy out of the fiber.

The energy measured coming out of the SLTD fibers as a function of the energy measured going into the SLTD light tube assembly is shown in Fig. 3(b). The relationship is linear, with an offset due to a ~ 11 nJ background, likely from low levels of stray light. The slope ($5.93 \pm 0.41 \times 10^{-7}$) was taken to be the transmission at 532 nm. Each of the fiber ports measured the same transmission to within 5%. This calibration has been applied to all SLTD units, which are nominally identical.

Calibration of other SLTD components, including the filters and photodiodes, was conducted individually using wavelength-tunable continuous sources between 300 and 800 nm. These measurements demonstrate that the flattening filter reduced the wavelength dependence of the total SRS sensitivity, resulting in a standard deviation of 4% to 9% over the SRS wavelength range. The relative wavelength dependence of the diffuser transmission was confirmed with measurements showing that the transmission at 635 nm is 1.06 ± 0.01 of the transmission at 532 nm, consistent with the nominal value of 1.07.

The photometrics for the three channels, at the appropriate wavelengths, are summarized in Table II with the signal given by:

$$\text{Signal}(V) = F * [T_{LT} T_{coll} T_{filt} S_{diode} R_{scope} \Omega_{SLTD}], \quad (1)$$

where F is the incident fluence (W/sr), T are the transmission of the light tube, collimator, and filters, S_{diode} is the diode sensitivity (A/W), R_{scope} is the digitizer impedance (50 Ω), and Ω_{SLTD} is the diffuser solid angle as viewed from TCC, $\sim 5.8 \times 10^{-5}$ sr. The light tube assembly transmission is based on the calibration at 532 nm (Fig. 3), extrapolated to 351 nm and 702 nm by the nominal wavelength dependence of the diffuser transmission. The overall absolute energy response of SLTD is contained in the photodiode calibration, as most other terms in Eq. 1 are unitless or fixed. For a comprehensive wavelength-dependent calibration, a bright wavelength-tunable source is desired to measure the SLTD transmission as a function of wavelength between 350 and 750 nm. The filter transmission includes the collimator, bandpass filters, and the SRS channel flattening filter. The total integrated sensitivity of the SLTD channels, before accounting for ND filtering, is computed to be around

TABLE II. SLTD component and integrated sensitivity (V per W/sr incident on SLTD) at representative wavelengths for each channel. The integrated sensitivity is the product of the sensitivity of each component, and the $50\ \Omega$ impedance in the digitizer, divided by the solid angle of 5.8×10^{-5} sr. ND filters, used in some channels, are not included in this calculation.

Channel (λ)	Light tube transmission	Collimator/filter transmission	Photodiode sensitivity (mA/W)	Integrated sensitivity [V/(W/sr)]
SBS (351 nm)	5.09×10^{-7}	0.40	65	3.9×10^{-11}
SRS (430-760 nm)	5.93×10^{-7}	0.083	27	3.9×10^{-12}
$\omega/2$ (695-735 nm)	6.55×10^{-7}	0.85	6.5	1.1×10^{-11}

3.9×10^{-11} V/(W/sr) for SBS, 3.9×10^{-12} V/(W/sr) for SRS, and 1.1×10^{-11} V/(W/sr) for $\omega/2$.

IV. NIF DATA

The first six SLTD units have collected data on a variety of NIF shots, including direct-drive and indirect-drive ICF and high-energy-density physics experiments. These units are located at (θ, ϕ) port angles of (7,225), (18,213.75), (36.75,94), (36.75,274), (56,113), and (90,164) degrees. A collection of sample data from the (18,213.75) degrees unit is shown in Fig. 4, including SBS signal from PDD shot N200715-002, SRS signal from indirect-drive shot N200727-001, and $\omega/2$ signal from x-ray diffraction shot N191016-001. This data does not correct for distortion in the electrical cables. The data demonstrate that requirements on temporal resolution and dynamic range or signal to noise are satisfied. The 10% to 90% rise of the signal occurs over no more than three 0.32-ns time samples, corresponding to a resolution of better than 1 ns. The noise floor consists of intrinsic electrical noise with an amplitude around ~ 0.5 mV. For signals larger than ~ 200 mV, the digitization noise increases with signal at a signal-to-noise level of up to ~ 500 , signifying an effective dynamic range equivalent to ~ 9 bits. The absolute timing of the SLTD trace relative to the laser pulse is currently based on correlation of the rising (falling) edge of signals with the rising (falling) edge of the laser pulse over many shots. An absolute timing fiducial may be implemented to confirm this.

SLTD data can be used to map out the angular dependence of the scattered-light distribution. An example of the SBS data from PDD shot N200715-002 is shown in Fig. 5. Error bars are the quadrature sum of uncertainties in the factors comprising the overall calibration of the SBS channel, including a $\pm 6.9\%$ uncertainty in the light tube transmission, $\pm 4.0\%$ in the collimator transmission, $\pm 3.8\%$ in the filter transmission, and $\pm 1.6\%$ in the photodiode sensitivity, for a total systematic uncertainty of $\pm 9.0\%$. The relative, port-to-port uncertainty is lower. The statistical uncertainty depends on signal to noise levels and varies from shot to shot, but is generally $< \pm 5\%$. The measured SBS-band light can be used to evaluate the angular distribution in *SAGE*¹⁷ calculations of unabsorbed light through a 3D laser ray-trace

with inverse bremsstrahlung absorption, scaled to match the data points around 37° . The data agree qualitatively with a peak near 30° , though the angular variation evidenced by the shape of the curve shows quantitative differences that will be explored in future work.

V. CONCLUSIONS

In summary, the absolutely calibrated NIF SLTD suite is being implemented to diagnose time-resolved scattered light in three wavelength bands corresponding to SBS (~ 351 nm), SRS (430 to 760 nm), and $\omega/2$ (695 to 745 nm) light. Six units have collected data, validating the instrument temporal resolution, sensitivity, and signal to noise ratio. SLTD was calibrated by offline measurements of the transmission and sensitivity of optical components, including the integrated light tube assembly, collimators, filters, and photodiodes. Comparison of absolute SLTD scattered-light energy measurements to FABS is ongoing, and calibration experiments to validate SBS and SRS measurements are planned. The remaining nine SLTD units will be implemented at port locations between $\theta = 63^\circ$ and 143° . The data will constrain models of laser energy coupling and laser-plasma instabilities in direct-drive and indirect-drive ICF experiments.

ACKNOWLEDGMENTS

The authors thank the NIF operations and facility crews for their assistance in installing and qualifying these instruments. This material is based upon work supported by the Department of Energy National Nuclear Security Administration under Award Number DE-NA0003856 and under contract DE-AC52-07NA27344, the University of Rochester, and the New York State Energy Research and Development Authority.

This report was prepared as an account of work sponsored by an agency of the U.S. Government. Neither the U.S. Government nor any agency thereof, nor any of their employees, makes any warranty, express or implied, or assumes any legal liability or responsibility for the accuracy, completeness, or usefulness of any information, apparatus, product, or process disclosed, or represents that its use would not infringe privately owned rights.

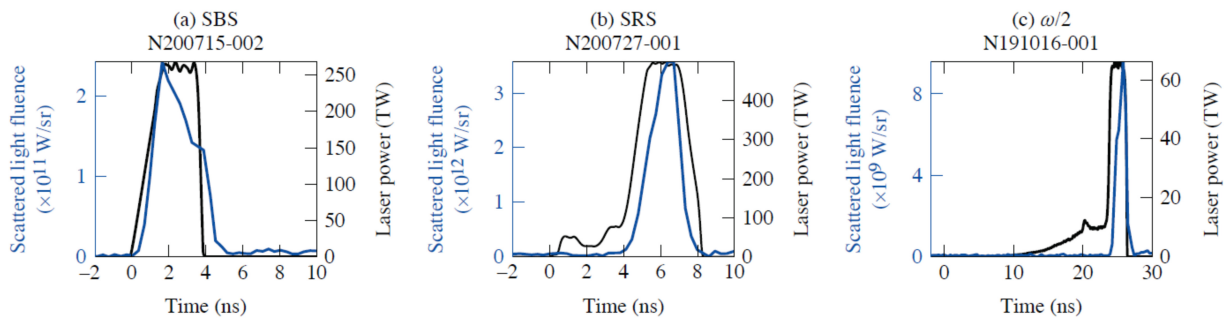


FIG. 4. Sample SLTD data obtained at (18,213.75) on different NIF experiments in the (a) SBS, (b), SRS, and (c) $\omega/2$ channels. The SLTD signal trace (blue) is overlaid with the total laser power (black).

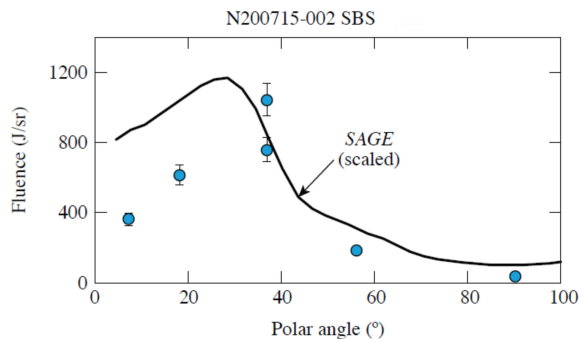


FIG. 5. Measured SBS scattered-light distribution (points) on PDD exploding-pusher shot N200715-002 in comparison to the scaled SAGE-simulated unabsorbed-light distribution (line). The simulation is scaled by a factor of 0.28 to roughly match the points at 37° .

Reference herein to any specific commercial product, process, or service by trade name, trademark, manufacturer, or otherwise does not necessarily constitute or imply its endorsement, recommendation, or favoring by the U.S. Government or any agency thereof. The views and opinions of authors expressed herein do not necessarily state or reflect those of the U.S. Government or any agency thereof.

VI. DATA AVAILABILITY

The data that support the findings of this study are available from the corresponding author upon reasonable request.

¹W. L. Kruer, *The physics of laser plasma interactions* (Addison-Wesley, Redwood City, CA, 1988).

²S. Atzeni and J. Meyer-Ter-Vehn, *The Physics of Inertial Fusion: Beam Plasma Interaction, Hydrodynamics, Hot Dense Matter*, International Series of Monographs on Physics (Clarendon, Oxford, 2004).

³J. F. Drake, P. K. Kaw, Y. C. Lee, G. Schmid, C. S. Liu, and M. N. Rosenbluth, *The Physics of Fluids* **17**, 778 (1974), <https://aip.scitation.org/doi/pdf/10.1063/1.1694789>.

⁴R. S. Craxton, K. S. Anderson, T. R. Boehly, V. N. Goncharov, D. R. Harding, J. P. Knauer, R. L. McCrory, P. W. McKenty,

D. D. Meyerhofer, J. F. Myatt, *et al.*, *Physics of Plasmas* **22**, 110501 (2015).

⁵J. Lindl, *Phys. Plasmas* **2**, 3933 (1995).

⁶C. S. Liu, M. N. Rosenbluth, and R. B. White, *Physics of Fluids* **17**, 1211 (1974).

⁷A. Simon, R. W. Short, E. A. Williams, and T. Dewandre, *Physics of Fluids* **26**, 3107 (1983).

⁸C. A. Haynam, P. J. Wegner, J. M. Auerbach, M. W. Bowers, S. N. Dixit, G. V. Erbert, G. M. Heestand, M. A. Henesian, M. R. Hermann, K. S. Jancaitis, K. R. Manes, C. D. Marshall, N. C. Mehta, J. Menapace, E. Moses, J. R. Murray, M. C. Nostrand, C. D. Orth, R. Patterson, R. A. Sacks, M. J. Shaw, M. Spaeth, S. B. Sutton, W. H. Williams, C. C. Widmayer, R. K. White, S. T. Yang, and B. M. V. Wonterghem, *Appl. Opt.* **46**, 3276 (2007).

⁹J. D. Moody, P. Datte, K. Krauter, E. Bond, P. A. Michel, S. H. Glenzer, L. Divol, C. Niemann, L. Suter, N. Meezan, *et al.*, *Review of Scientific Instruments* **81**, 10 (2010).

¹⁰R. L. Berger, C. A. Thomas, K. L. Baker, D. T. Casey, C. S. Goyon, J. Park, N. Lemos, S. F. Khan, M. Hohenberger, J. L. Milovich, D. J. Strozzi, M. A. Belyaev, T. Chapman, and A. B. Langdon, *Physics of Plasmas* **26**, 012709 (2019), <https://doi.org/10.1063/1.5079234>.

¹¹P. Michel, L. Divol, E. L. Dewald, J. L. Milovich, M. Hohenberger, O. S. Jones, L. Berzak Hopkins, R. L. Berger, W. L. Kruer, and J. D. Moody, *Phys. Rev. Lett.* **115**, 055003 (2015).

¹²M. J. Rosenberg, A. A. Solodov, J. F. Myatt, W. Seka, P. Michel, M. Hohenberger, R. W. Short, R. Epstein, S. P. Regan, E. M. Campbell, T. Chapman, C. Goyon, J. E. Ralph, M. A. Barrios, J. D. Moody, and J. W. Bates, *Phys. Rev. Lett.* **120**, 055001 (2018).

¹³P. Michel, M. J. Rosenberg, W. Seka, A. A. Solodov, R. W. Short, T. Chapman, C. Goyon, N. Lemos, M. Hohenberger, J. D. Moody, S. P. Regan, and J. F. Myatt, *Phys. Rev. E* **99**, 033203 (2019).

¹⁴M. Hohenberger, P. B. Radha, J. F. Myatt, S. LePape, J. A. Marozas, F. J. Marshall, D. T. Michel, S. P. Regan, W. Seka, A. Shvydky, *et al.*, *Physics of Plasmas* **22**, 056308 (2015), <http://aip.scitation.org/doi/pdf/10.1063/1.4920958>.

¹⁵W. A. Farmer, O. S. Jones, M. A. Barrios, D. J. Strozzi, J. M. Koning, G. D. Kerbel, D. E. Hinkel, J. D. Moody, L. J. Suter, D. A. Liedahl, N. Lemos, D. C. Eder, R. L. Kauffman, O. L. Landen, A. S. Moore, and M. B. Schneider, *Plasma Physics and Controlled Fusion* **60**, 044009 (2018).

¹⁶J. A. Marozas, M. Hohenberger, M. J. Rosenberg, D. Turnbull, T. J. B. Collins, P. B. Radha, P. W. McKenty, J. D. Zuegel, F. J. Marshall, S. P. Regan, T. C. Sangster, W. Seka, E. M. Campbell, V. N. Goncharov, M. W. Bowers, J.-M. G. Di Nicola, G. Erbert, B. J. MacGowan, L. J. Pelz, and S. T. Yang, *Phys. Rev. Lett.* **120**, 085001 (2018).

¹⁷R. S. Craxton and R. L. McCrory, *Journal of Applied Physics* **56**, 108 (1984), <https://doi.org/10.1063/1.333742>.